Electronic Supplementary Information (ESI)

Understanding the role of supported Rh atoms and clusters during hydroformylation and CO hydrogenation reaction with i*n situ*/*operando* XAS and DRIFT spectroscopy

Bidyut Bikash Sarma,[1,2,3*] Dominik Neukum,[2] Dmitry E. Doronkin,[1,2] Ajai Raj Lakshmi Nilayam,[4] Lorena Baumgarten,[1,2] Bärbel Krause,[5] and Jan-Dierk Grunwaldt[1,2]

[1]Institute for Chemical Technology and Polymer Chemistry, Karlsruhe Institute of Technology (KIT), Engesserstraße 20, 76131 Karlsruhe, Germany

[2]Institute of Catalysis Research and Technology, KIT, Hermann-von Helmholtz Platz 1, 76344 Eggenstein-Leopoldshafen, Germany

[3]Laboratoire de Chimie de Coordination (LCC), CNRS, Université de Toulouse, INPT, 205 route de Narbonne, 31077 Toulouse Cedex 4, France

[4]Institute of Nanotechnology, KIT, Hermann-von-Helmholtz Platz 1, 76344 Eggenstein-Leopoldshafen, Germany

[5]Institut für Photonenforschung und Synchrotronstrahlung (IPS), KIT, Hermann-von-Helmholtz Platz 1, D-76021 Karlsruhe, Germany

Email: bidyut-bikash.sarma@lcc-toulouse.fr; bidyutbikash.sarma@toulouse-inp.fr

Experimental

1.1. Materials

Metal precursors $Rh(acac)_3$ (Sigma-Aldrich, 97%), $[(C_6H_5)_3P]_3Rh(CO)H$ (Sigma Aldrich, 97%), $Rh(NO_3)_3 \cdot xH_2O$ (Sigma Aldrich, 36% Rh basis), $Ce(NO_3)_3 \cdot 6H_2O$ (Sigma Aldrich, 99% trace metal basis), $Mg(NO_3)_2 \cdot 6H_2O$, (Alfa Aesar, 98%), $ZrO(NO_3)_2 \cdot xH_2O$ (Sigma-Aldrich, 99%), Cerium(III) 2-ethylhexanoate, (Alfa Aesar, 49% in 2-ethylhexanoic acid, Ce 12%), Xylene (Sigma Aldrich, 99%) were used as received. Potassium hydroxide (KOH) and ethanol were purchased from EMPLURA®. Gas mixtures such as 99.99% ethylene, 99.99% CO, 99.99% H_2, 99.9% N_2, 10% CO/Ar, 20% O_2/Ar, 10% H_2/Ar and pure Ar (99.999%) bottles were purchased from Air Liquide.

1.2 Catalyst synthesis

(a) **Preparation of ceria support**: The ceria support was prepared by two different methods (a) calcination of cerium nitrate hexahydrate precursor at 623 K (ramp rate 2 K/min) under static air for 5 h and (b) precipitation of cerium nitrate hexahydrate under basic condition (1M KOH, pH=10) followed by calcination at 623 K (ramp rate 2 K/min) under static air for 5 h.

(b) **Preparation of Rh catalysts by wet impregnation:** Rh catalysts were synthesized over ceria support by wet impregnation (WI) and precipitation (PP) methods similar to our previous work.[1] For the wet impregnation method, acetylacetonate precursors of the metals were first dissolved in acetone and then dispersed over ceria (synthesis procedure explained in (a)). The solution was sonicated for 5 min and evaporated to dryness under vacuum in a rotary evaporator. The impregnates were further dried in an oven overnight at 353 K in static air. The solids were afterwards ground, mixed with mortar and pestle, and finally calcined at 1073 K under static air.

(c) **Preparation of Rh catalysts by precipitation**: For catalysts synthesized via precipitation, Rh $(NO_3)_3$ and $Ce(NO_3)_2$/$ZrO(NO_3)_2$/$Mg(NO_3)_2$ salts were first dissolved in water and the pH value of the solution was increased to 10 by adding 1 M KOH solution over a period of 3 h under continuous stirring. At pH 10, the solutions were further kept stirring for another 30 min to achieve a stable pH. The slurry was then transferred into a closed glass vessel and kept at 353 K overnight. The solid fractions were centrifuged and washed with distilled water (3 times) followed by ethanol (3 times). The solid was further dried at 353 K for 12 h and ground to fine powder with mortar and pestle. The solid was then calcined at 623 K (ramp rate 2 K/min) under static air for 5 h under static air. For ZrO_2 and MgO supported catalysts, the calcination temperature was 773 K.

(d) **Preparation of Rh catalysts by flame spray pyrolysis (FSP):** Double flame spray pyrolysis (DFSP) was used in a double-nozzle FSP setup (Figure S8b). The nozzles were separated by 10 cm with an angle of 120°. Appropriate amounts of $Rh(acac)_3$ (1wt% Rh) and Cerium(III) 2-ethylhexanoate (49% in 2-ethylhexanoic acid) were dispersed in xylene and sonicated for 30 minutes. The solution was sprayed

over the two nozzles at a rate of 5 mL/min using two syringe pumps. Each flame was ignited by a pre-mixed CH_4 flame (1.6 L/min of O_2 and 750 mL/min of CH_4). Pure oxygen was used as dispersion gas (5 L/min) at a 0.3 MPa pressure drop. All the gas flows were controlled by mass flow controllers. The particles were collected on glass fiber filters (24 cm diameter, Whatman GF6) in a water-cooled round holder connected to a vacuum pump. The solid was further calcined at 623 K in air (ramp rate of 2 K/min) for 5 h.

(e) **Rh catalyst prepared via pyrolysis**: Appropriate amount of $[(C_6H_5)_3P]_3Rh(CO)H$ (1 wt% Rh) is dissolved in acetone and dispersed over ceria powder (1g) synthesized by precipitation method. The solution was evaporated to dryness under vacuum in a rotary evaporator. The solid was further dried in an oven at 353 K overnight. The resulting solid was ground to fine powder with mortar and pestle and pyrolyzed at 973 K under Ar (flow of 100 mL/min) for 1 h with a ramp rate of 10 K/min.

1.3. Characterization of the catalysts

1.3.1. ***Powder X-ray diffraction (XRD):*** PANalytical X'Pert Pro instrument was used to measure the powder X-ray diffraction patterns of the catalysts using a Bragg-Brentano geometry with Cu−Kα radiation (1.54060 Å) and a Ni filter. Si wafer holder was used to mount the catalysts. The diffractograms were collected from 20° to 80° (2θ) for a total time of 8 h at room temperature (step size of 0.017°, 0.53 s acquisition time, 5 scans). The JCPD (Joint Committee of Powder Diffraction) standards database was used to compare the reflection patterns.

1.3.2. H*igh-angle annular dark field scanning transmission electron microscopy (HAADF-STEM):* HAADF-STEM images were acquired using an aberration (probe) corrected Themis 300 (Thermo Fischer Scientific) microscope operated at 300 kV (convergence angle: 30 mrad, collection angle: 77-200 mrad). Finely ground powder samples were dry-cast on standard lacey carbon grid with Cu mesh. The excess powder was removed with a dust-off gun. Energy dispersive X-ray (EDX) maps were acquired with Super-X EDX detector.

1.3.3. ***X-ray absorption spectroscopy:*** X-ray absorption spectra at the Rh K-edge (23220 eV) were collected at the P65 beamline of the Deutsches Elektronen-Synchrotron (DESY), Hamburg, Germany[2] and at the CATACT beamline of the KIT Light Source, Karlsruhe, Germany.[3] To scan the incident energy, a Si (311) double crystal monochromator (DCM) was used. For measuring the reference samples, pellets diluted with cellulose were used, and the measurements were conducted in transmission. For *ex-situ* measurements, the catalysts were kept inside a quartz capillary micro reactor without dilution and the measurements were conducted in fluorescence mode as reported in our previous work.[1] The processing of the XAS results (data reduction and fitting) was carried out using the Demeter software package.[4] Data treatment (alignment, normalization) has been performed using the Athena code (version 0.9.26. A model based on standard crystallographic data was used to fit the experimental data. For all

fits, k value up to 12 Å^{-1} and radial distance (R) between 1-3.5 Å were considered. S_0^2 was derived from the corresponding metallic Rh foil reference spectra to determine the coordination number. The EXAFS equation[5] used for deriving the free parameters is given by

$$\chi(k) = S_o^2 \sum_i N_i \frac{f_i(k)}{kR_i^2} \; e^{-\frac{2R_i}{\lambda(k)}} \; e^{-2k^2\sigma_i^2} \; sin(2kR_i + \delta_i(k))$$

where S_o^2 represents amplitude reduction factor (estimated from the fit of Ru foil), N is the degeneracy of the scattering path (fitted), f(k) is the scattering function (calculated using FEFF 6[6]), k is the wavenumber, R is the distance between absorber and scatterer (fitted), λ is the mean free path of the photoelectron (calculated using FEFF 6), σ^2 is the mean square radial displacement, also known as the Debye-Waller factor (fitted), δ is the phase shift of the couple absorber/scatterer, (calculated using FEFF 6) and i represents a particular number of shell. R-factor that is frequently used while reporting quality of fit; represents goodness of the fit.

For *in-situ* XAS measurements, catalyst sieved fraction (100-200 μm) was used and filled in a quartz capillary micro reactor (2 mm outer diameter, 0.02 mm wall thickness). Gas mixtures (99.99% ethylene, 99.99% CO and 99.99% H_2) were fed through the capillary with a flow of 30 mL/min with the help of mass flow controllers. For temperature programmed reduction experiments, the samples were heated to the required temperature with a gas blower (Leister LE mini kit at DESY). For the high-pressure experiments at 10 bar, same set up was used with an additional back pressure regulator. Online analysis of the gas mixtures was carried out qualitatively with a mass spectrometer (Pfeiffer Vacuum OmniStar GSD-320). Mass fragments of 2 (H_2), 27 and 28 (ethylene), 28 and 16 (CO), 31 and 32 (CH_3OH), 45 and 46 (C_2H_5OH) and 57 and 58 (C_3H_6O) were monitored. Linear combination fitting (LCF) was conducted to derive the fraction of oxidic and reduced species during temperature-dependent XAS studies. The fitting was performed by using the first and the last spectra from the respective dataset as internal references within the energy range of 23200-23250 eV.

1.3.4 X-Ray Photoelectron Spectroscopy (XPS): X-Ray Photoelectron Spectra were measured with a SPECS Phoibos 150 analyser using a non-monochromatic XR-50 Mg Kα X-ray source, an angle of 45° between analyser and sampler, illuminating an area with a Full width half maximum (FWHM) of 2 mm (circular spot). Effects from sample charging were minimized with a flood gun. The energy scale was calibrated with an Ag reference. High resolution spectra were taken with a pass energy of the analyser of 20 eV. Data processing was conducted using CasaXPS software. The energy scale of all spectra was referenced to the 1s peak of graphitic carbon (284.8 eV). FWHM of Rh^{3+} species fixed at 2.1 ± 0.1 eV and FWHM of Rh^0 species fixed at 1.7 ± 0.2 eV. Area ratio of 3:2 for 5/2 and 3/2 peaks, shifted by a fixed delta of 4.75 eV. After Shirley background subtraction the spectra were fitted. For the deconvolution of the individual oxidation states in the Rh 3d spectra, initial constraints were chosen in

accordance with the literature.[7,8,9,10] The constraints were optimized until the best agreement of the fitting function was achieved for all samples of this study.

1.3.4. *In-situ diffuse reflectance infra-red spectroscopy*: *In-situ* DRIFTS experiments were conducted on a VERTEX 70 FTIR spectrometer from Bruker. A Harrick Praying Mantis optics and the Harrick high temperature cell with a flat CaF_2 window were used. A sieve fraction of 100-200 µm of the catalyst was used for the measurements. All the catalysts were pre-treated by purging with He or Ar and heating to 573 K for 1 h to remove any impurity adsorbates from the catalyst surface. The resulting spectra were collected in reflectance mode between 1000-4000 cm^{-1} under the reaction mixture. A 4 cm^{-1} spectral resolution was used for all measurements. Spectra were collected at various temperature, and the working setpoint of the heater was selected based on a calibration performed via a thermal imaging IR camera (ImageIR 8300 from Infratec) as shown in the supporting information, figure S21. The spectra are reported in logarithm log(1/R) or in Kubelka-Munk units by converting with the following formula

$$F(R_\infty) = \frac{(1 - R_\infty)^2}{2R_\infty}$$

where R_∞ stands for reflectance of the sample (measured relative to the sample under Ar at the respective temperature as a background scan).

For the background spectra, 200 scans were collected and averaged under Ar flow and for the samples 150 scans were collected per measurement. The measurements were performed continuously over a range of 0.5-1 h. The gas mixture at the outlet of the *in-situ* cell was qualitatively analyzed by an online mass spectrometer (Pfeiffer Vacuum OmniStar GSD-320).

1.3.5. *Quantification of metal content*: Quantitative analysis of the metal content of the catalysts was performed by ICP-OES measurements (Agilent 720/725-ES instrument). For this, 30-40 mg of the samples were digested in a mixture of sulfuric and nitric acid (1:1) in a microwave digestion system at 453 K for 45 min.

1.3.6. *N_2-physisorption*: All the nitrogen physisorption isotherms were recorded at 77 K using a Rubotherm BELSORP-mini II instrument. The specific surface areas were determined by the Brunauer–Emmett–Teller (BET) method. Catalysts were degassed at 423 K for 2 h under vacuum prior to the measurement.

1.3.7. H_2-Temperature Program Reduction (TPR): The TPR measurements were carried out in a quartz reactor. 150-200 mg of catalyst powder were loaded and heated under Ar up to 573 K (ramp rate 10 K/min) for 1 hour to remove any impurity adsorbate from the catalyst surface. Afterward, the reactor is cooled down to 313 K and 10% H_2/Ar was introduced as gas mixture. The outlet of the reactor is connected to a thermal conductivity detector (TCD) to monitor the H_2 consumption. A H_2O trap is placed before the detector, which is cooled with liquid nitrogen during the measurement.

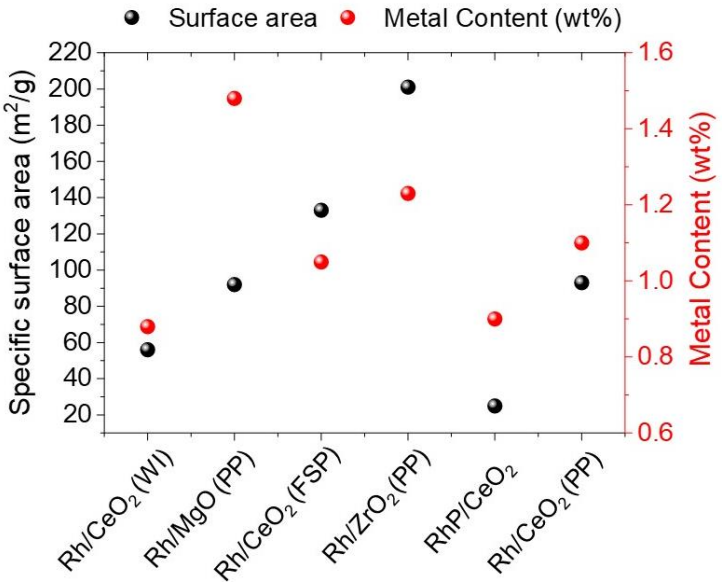

Figure S1. Plot of BET specific surface area derived from N_2 physisorption isotherms of Rh catalysts synthesized via various methods versus the metal content obtained from ICP-OES analysis. WI, FSP and PP stands for wetness impregnation, flame spray pyrolysis and precipitation respectively.

Table 1. The value of BET specific surface area derived from N_2 physisorption isotherms of Rh catalysts synthesized via various methods and the metal content obtained from ICP-OES analysis.

Catalyst	Metal content (wt%)	Specific Surface Area (BET), m^2/g
Rh/CeO_2 (WI)	0.88	56
Rh/MgO (PP)	1.48	92
Rh/CeO_2 (FSP)	1.05	133
Rh/ZrO_2 (PP)	1.23	201
RhP/CeO_2	0.9	25
Rh/CeO_2(PP)	1.1	93

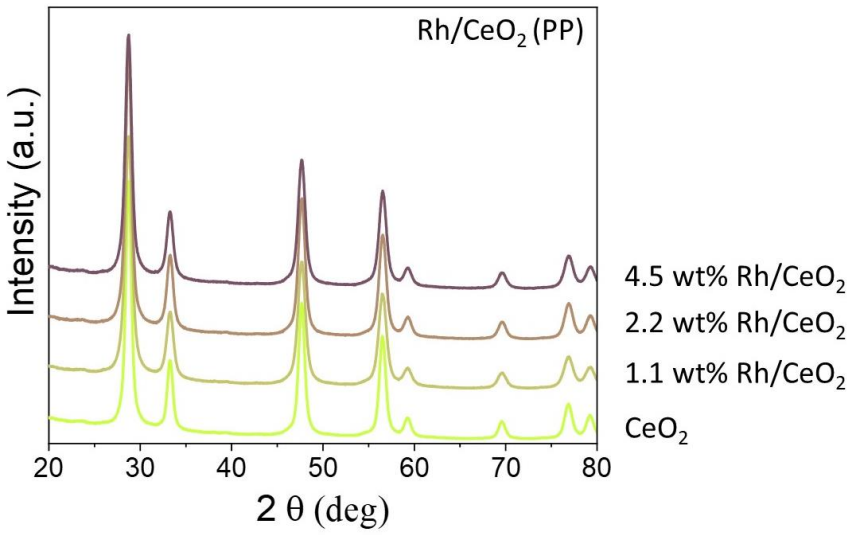

Figure S2. Powder XRD patterns of the Rh/CeO_2 catalysts (various concentrations) prepared via precipitation (PP) method and calcined at 623 K. For comparison, CeO_2 synthesized via same method is also shown.

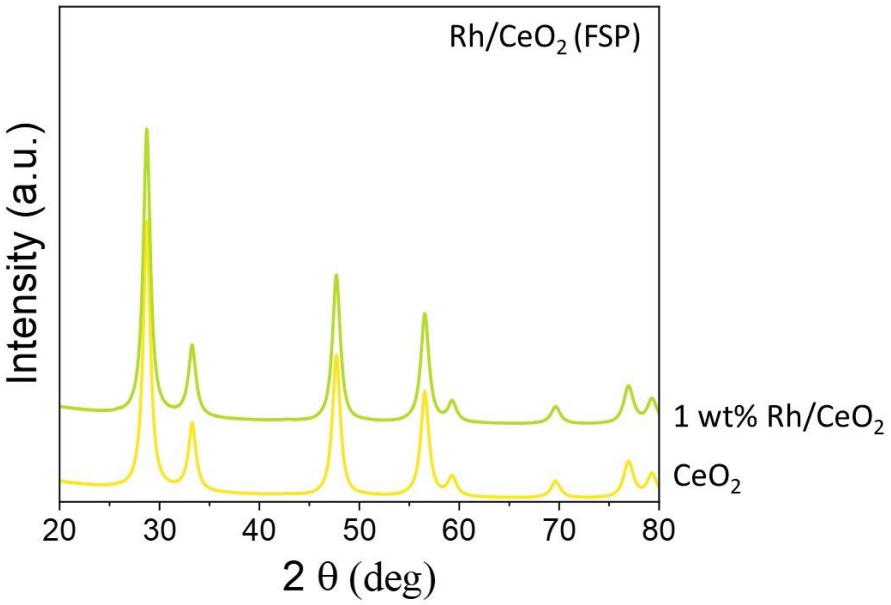

Figure S3. Powder XRD patterns of the Rh/CeO_2 catalysts prepared via flame spray pyrolysis (FSP) method and calcined at 623 K. For comparison, CeO_2 synthesized via same method is also shown at the bottom.

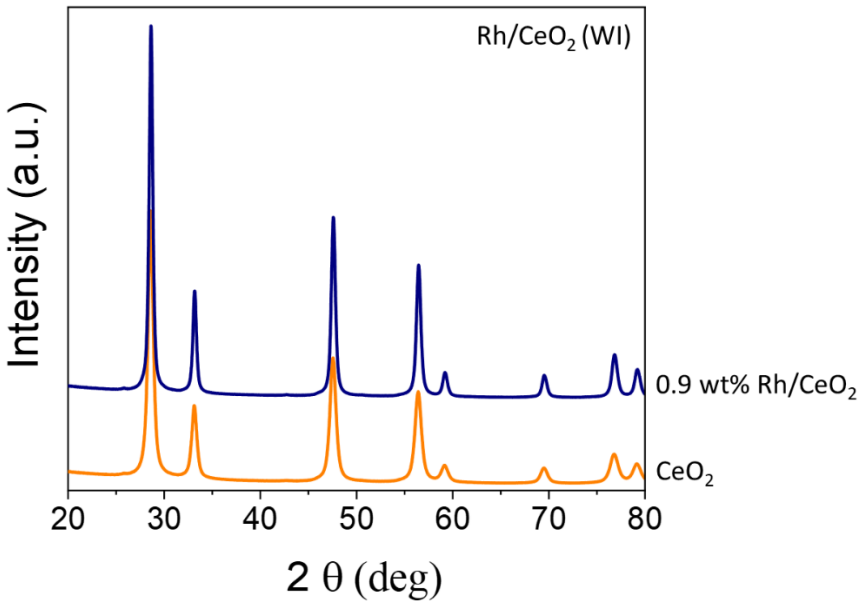

Figure S4. Powder XRD patterns of the Rh/CeO_2 (0.9 wt%) catalyst and CeO_2 support prepared via wet impregnation (WI) method and calcined at 1073 K.

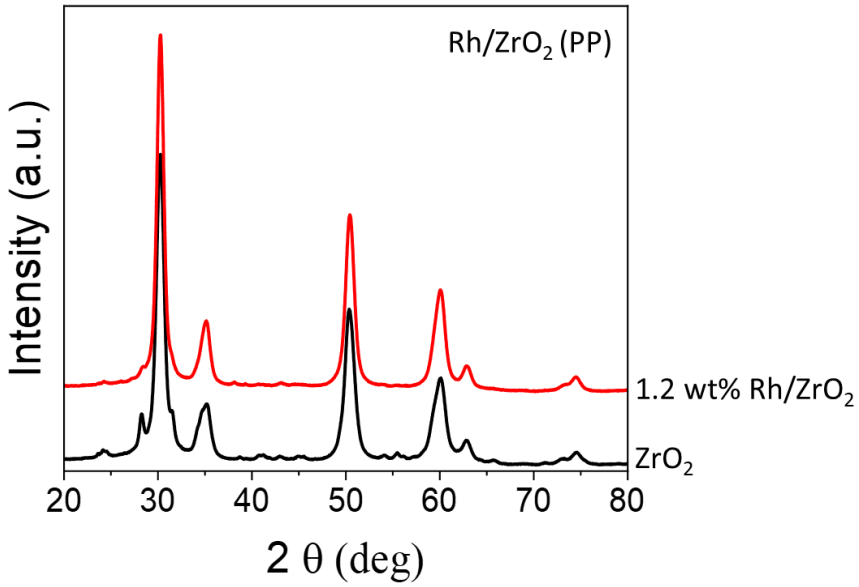

Figure S5. Powder XRD patterns of the Rh/ZrO_2 (1.2 wt%) catalyst and the bare ZrO_2 support prepared via precipitation method and calcined at 773 K. The reflection pattern corresponds to the tetragonal ZrO_2 phase.

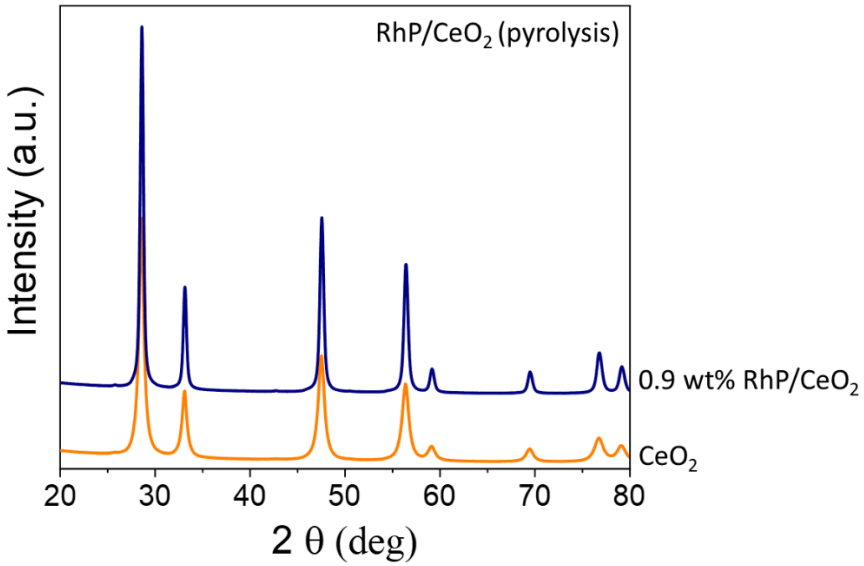

Figure S6. Powder XRD patterns of the RhP/CeO_2 catalyst prepared via anchoring molecular Rh complex $[(C_6H_5)_3P]_3Rh(CO)H$ over CeO_2 followed by pyrolysis at 973 K under Ar flow. For comparison, CeO_2 support pyrolyzed at same temperature is also shown.

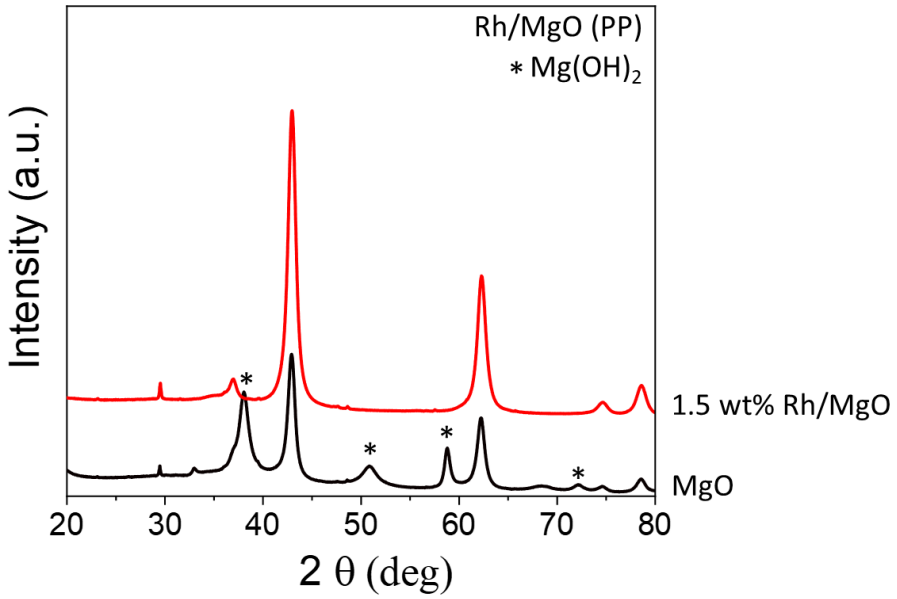

Figure S7. Powder XRD patterns of the Rh/MgO (1.5 wt%) catalyst prepared via the precipitation method and calcined at 773 K. The MgO support prepared via the same method is also shown. The asterisk (*) represents the contribution from the $Mg(OH)_2$ phase.

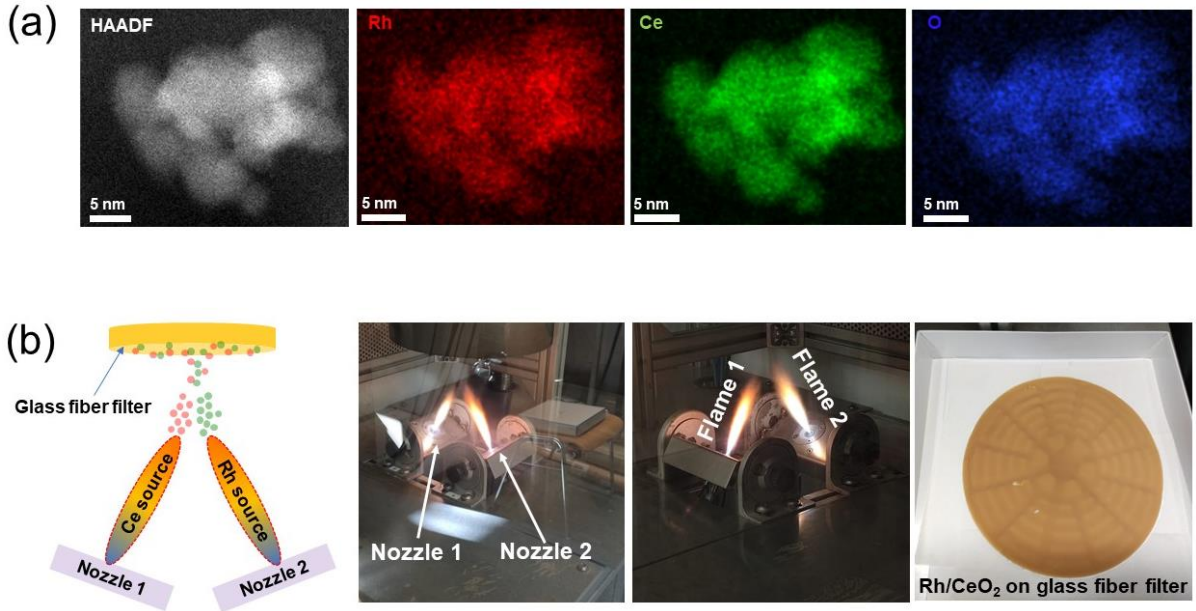

Figure S8. (a) HAADF-STEM images of Rh/CeO_2 catalyst synthesized via the flame spray pyrolysis (FSP) method and the corresponding EDX maps, (b) schematics and set up of Rh/CeO_2 catalyst synthesized via FSP method. Colour codes are rhodium : red, cerium : green and oxygen : blue respectively.

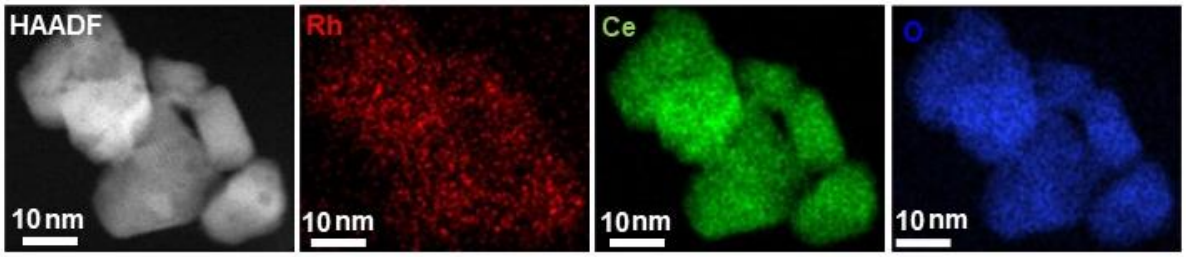

Figure S9. HAADF-STEM images of Rh/CeO_2 catalyst synthesized via wetness impregnation (WI) method and the corresponding EDX maps are shown. Colour codes are rhodium : red, cerium : green and oxygen : blue respectively.

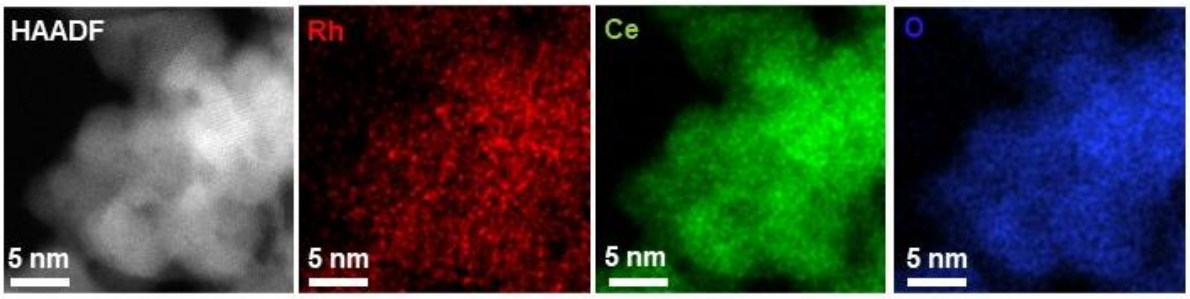

Figure S10. HAADF-STEM images of Rh/CeO_2 catalyst synthesized via the precipitation method and the corresponding EDX maps are shown. Colour codes are rhodium: red, cerium : green and oxygen : blue respectively.

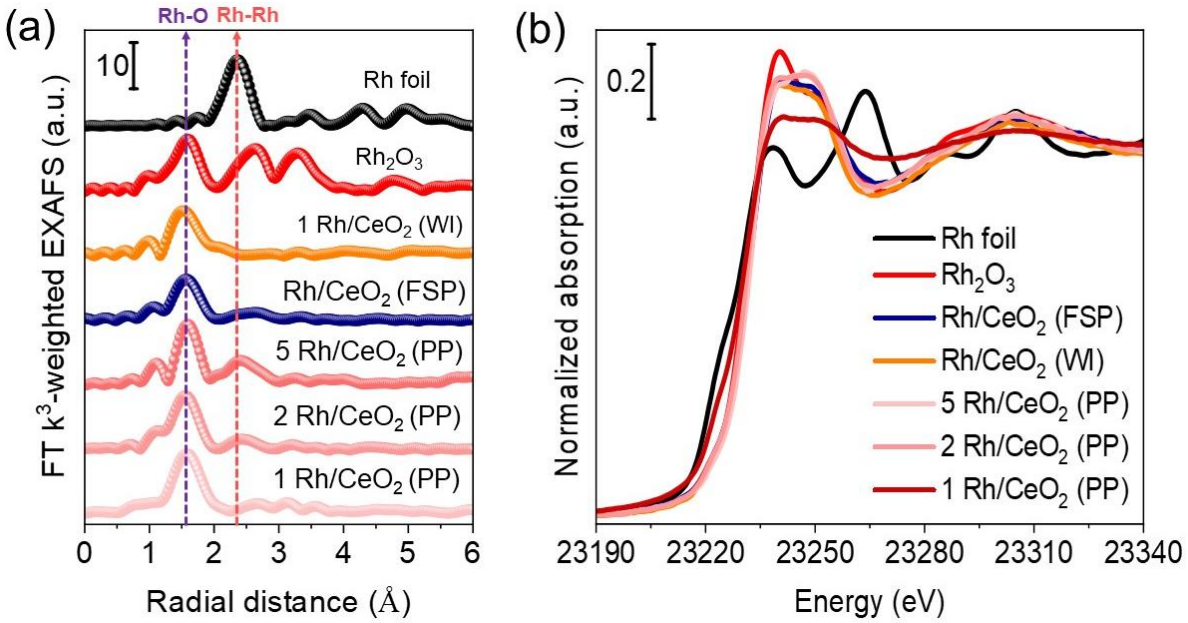

Figure S11. (a) Fourier transformed k^3-weighted EXAFS spectra and (b) XANES spectra at the Rh K-edge of the Rh catalysts supported over CeO_2 with various methods such as precipitation (PP), flame spray pyrolysis (FSP), and wet impregnation (WI). Rh_2O_3 and Rh foil are also shown as references for comparison.

Table S2. Structural parameters derived from EXAFS fitting. The k and radial distance (R) values considered for the fit were 3-11 $Å^{-1}$ and 1.0-2.1 Å respectively. Amplitude reduction factor, S_o^2 was derived from the fit of the metallic Rh foil. The value of S_o^2 was set to be 0.9. Crystallographic data of Rh_2O_3 (Coey 1970) was taken for the fit.

Catalyst	**Energy shift, E_o (eV)**	**Scattering path**	**CN**	**Radial distance, R (Å)**	**Debye Waller factor, $\sigma^2(Å^2)$**	**r-factor**
Rh/CeO_2 (PP)	-5.0 ± 1.6	Rh-O	4.5 ± 0.6	2.030 ± 0.012	0.0026 ± 0.0015	0.017
Rh/ZrO_2	-5.2 ± 3.8	Rh-O	4.2 ± 1.3	2.025 ± 0.026	0.0010 ± 0.0031	0.045
Rh/MgO	-4.1 ± 3.6	Rh-O	4.5 ± 1.2	2.051 ± 0.010	0.0019 ± 0.0025	0.049
Rh/CeO_2 (FSP)	-1.7 ± 1.9	Rh-O	4.3 ± 0.7	2.030 ± 0.015	0.0023 ± 0.0020	0.021
Rh/CeO_2 (WI)	-4.4 ± 2.2	Rh-O	3.9 ± 0.7	2.031 ± 0.009	0.0021 ± 0.0018	0.050

CN stands for coordination number and r-factor is goodness of fit.

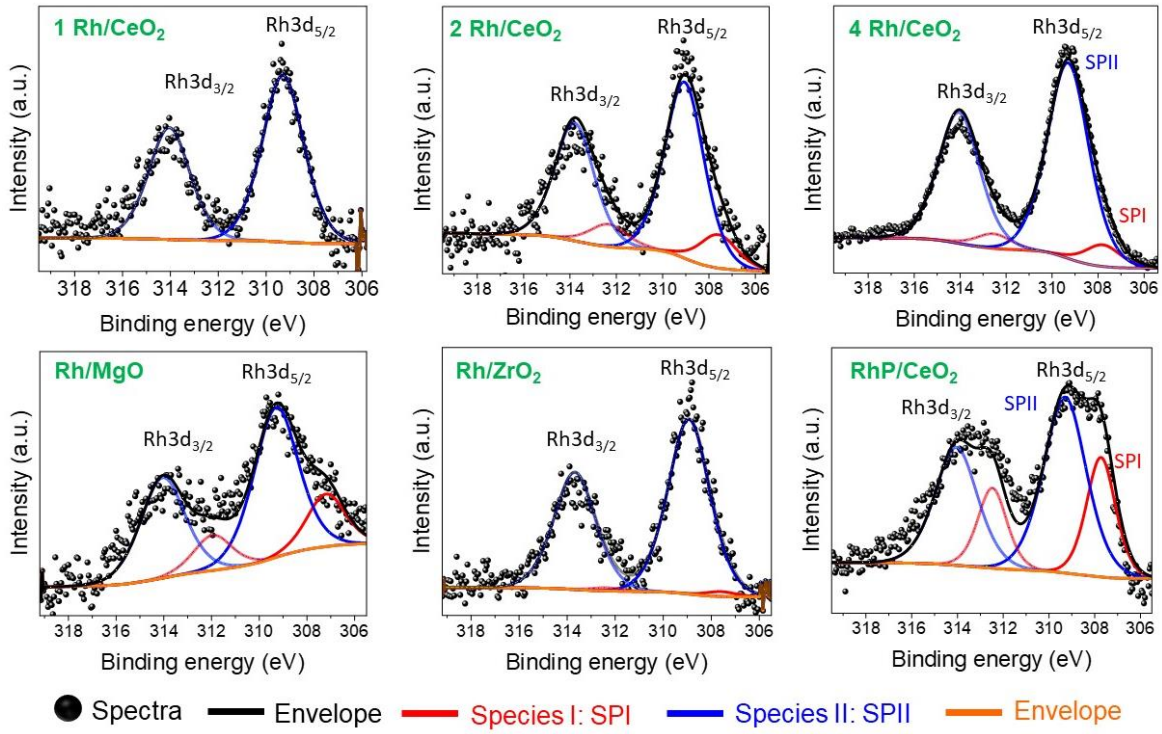

Figure S12. X-ray photoelectron spectra (XPS) of Rh catalysts in Rh 3d region synthesized via various methods over different support (CeO_2, MgO and ZrO_2). The table below shows different species, assignments and the corresponding percentage area.

Table S3. Component of Rh species, assignments and percentage are shown below.

Sample	Species (SP)	$Rh3d_{5/2}$ Binding Energy (eV)	Assignment	Area (%)
1.1% Rh/CeO_2	Species I	309.3	Rh^{III}	99
	Species II	307.4	Rh^0	1
2% Rh/CeO_2	Species I	309.3	Rh^{III}	98.6
	Species II	307.4	Rh^0	1.4
4.4% Rh/CeO_2	Species I	309.3	Rh^{III}	91.4
	Species II	307.8	Rh^0	8.6
2% Rh/MgO	Species I	309.2	Rh^{III}	78.1
	Species II	307.2	Rh^0	21.9
1.5% Rh/ZrO_2	Species I	308.1	Rh^{III}	98.5
	Species II	307.2	Rh^0	1.5
0.9% RhP/CeO_2	Species I	309.2	Rh^{III}	63.5
	Species II	307.8	Rh^0	36.5

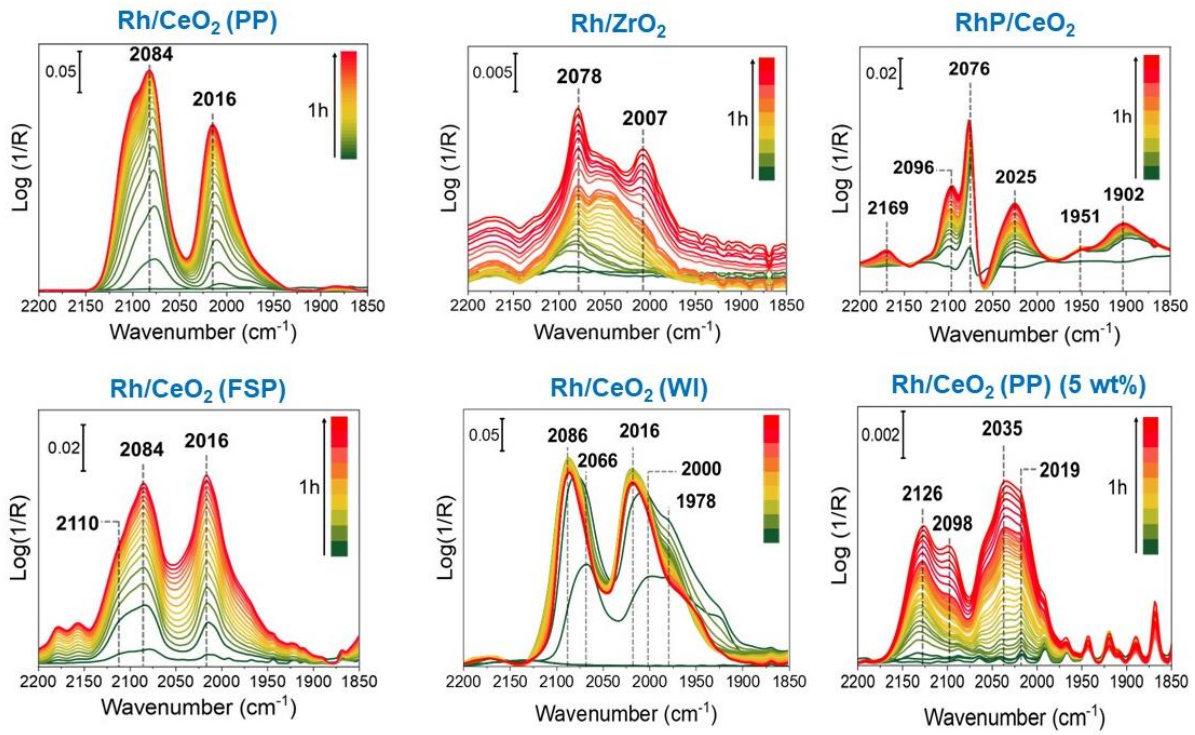

Figure S13. CO-DRIFT spectra (represented in logarithmic scale) at room temperature over various Rh catalysts. (a) Rh/CeO_2 (PP), (b) Rh/ZrO_2, (c) RhP/CeO_2, (d) Rh/CeO_2 (FSP), (e) Rh/CeO_2 (WI), and (f) 5 wt% Rh/CeO_2 (PP). PP: Precipitation, FSP: Flame Spray Pyrolysis, WI: Wet impregnation.

Table S4. CO absorption frequencies and their assignments over supported Rh catalysts. ν_s and ν_{as} represent symmetrical and asymmetrical stretching frequencies.

CO absorption frequency (cm^{-1})	Assignment	Support	Reference
2095 (ν_s), 2027 (ν_{as})	Geminal CO adsorbed to a Rh single atom	Al_2O_3	Ref[11]
2116-2120	Linear CO adsorbed to Rh^{2+}	Al_2O_3	Ref[12,13]
2102-2096 (ν_s) 2032-2022 (ν_{as})	Geminal CO adsorbed to a Rh^+ single atom	Al_2O_3	Ref[12]
2080-2100	Linear CO adsorbed to Rh^+	Al_2O_3	Ref[12,13]
2097 (ν_s), 2028 (ν_{as})	Geminal CO adsorbed to a Rh single atom	TiO_2	Ref[14, 15]
2110 (ν_s), 2039 (ν_{as})	Geminal CO adsorbed to a Rh^{3+} single atom	Phosphotungstic acid	Ref[16]
2100 (ν_s), 2039 (ν_{as})	Geminal CO adsorbed to a Rh^+ single atom	Phosphotungstic acid	Ref[16]
2102 (ν_s), 2036 (ν_{as})	Geminal CO adsorbed to a Rh^+ single atom	ZnO	Ref[17]
2114	Linear CO adsorbed to Rh^{3+}	CeO_2	Ref[1]
2120	CO adsorbed to Rh(O)	CeO_2	Ref[18]
2086 (ν_s), 2020 (ν_{as})	Geminal CO adsorbed to a Rh^+ single atom	CeO_2	Ref[1, 18]
2090 (ν_s), 2034 (ν_{as})	Geminal CO adsorbed to a Rh^+ single atom	CeO_2	Ref[19]
2056	Linear CO adsorbed over Rh (desorption of CO from $Rh(CO)_2$)	CeO_2	Ref[18]
2087, 2017	Geminal CO adsorbed to a Rh single atom	ZrO_2	Ref[20]
2105, 2032	Geminal CO adsorbed to a Rh single atom	CoO	Ref[21]
2110–2088 2045–2015	Geminal CO adsorbed to a Rh single atom	WO_x	Ref[22]
2101, 2032	Geminal CO adsorbed to a Rh single atom	Zeolite beta	Ref[23]
2154–2135	Linear CO adsorbed to a Rh^{3+} single atom	Zeolite MFI	Ref[24]
2125	Linear CO adsorbed to Rh^{2+}	Zeolite MFI	Ref[24]
2112 (ν_s), 2030 (ν_{as})	Geminal CO adsorbed to a Rh^+ single atom	Zeolite MFI	Ref[24]
2154-2158	Linear CO adsorbed to a Rh^{3+} single atom	Zeolite Y	Ref[25, 26]
2100-2090 (ν_s) 2035-2020 (ν_{as})	Geminal CO adsorbed to a Rh single atom	SiO_2	Ref[27]
2035	CO adsorbed to Rh-H	SiO_2	Ref[27]
2042-2076	Linear CO adsorbed to Rh^0	Al_2O_3	Ref[12, 28]
2000-2020	Bridged CO adsorbed to a Rh^+	Al_2O_3	Ref[12]
1900-1920	Bridged CO adsorbed to a Rh^0	Al_2O_3	Ref[12]

1800	Bridged CO adsorbed to a Rh^0	Al_2O_3	Ref[28]
2057	Linear CO adsorbed to Rh^0	CeO_2	Ref[l]
1850	Bridged CO adsorbed to a Rh^0	CeO_2	Ref[18]
2070	Linear CO adsorbed to Rh^0	ZnO	Ref[17]
1860	Bridged CO adsorbed to a Rh^0	ZnO	Ref[17]
2068	Linear CO adsorbed to Rh^0	TiO_2	Ref[14]
1860	Bridged CO adsorbed to a Rh^0	TiO_2	Ref[14]
1850	Bridged CO adsorbed to a Rh^0	ZrO_2	Ref[20]
2075	Linear CO adsorbed to Rh^0	Zeolite Y	Ref[25]

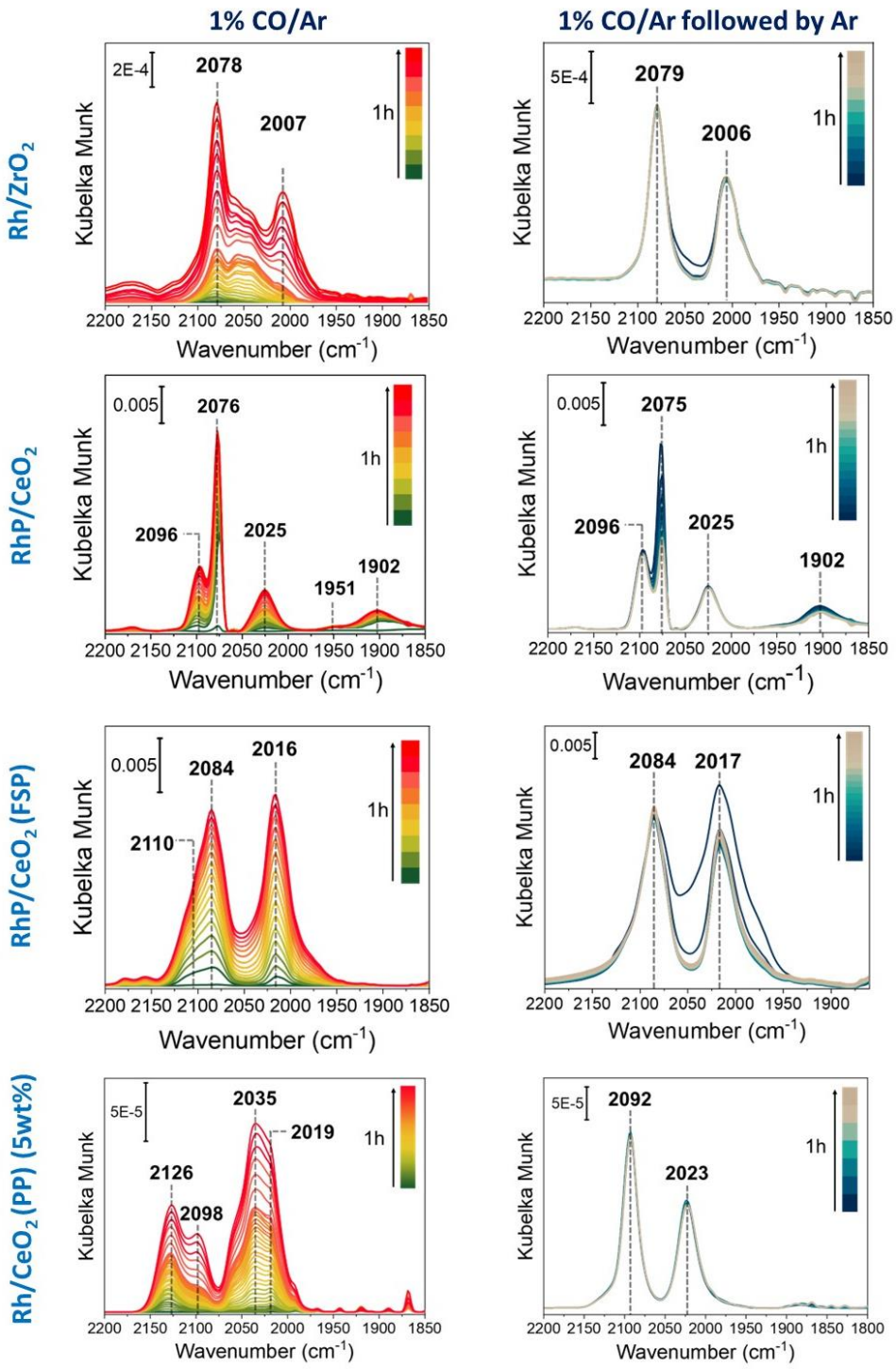

Figure S14. CO-DRIFTS spectra collected at room temperature over various Rh catalysts by flowing 1% CO/Ar (left) and followed by pure Ar (right) for 1 h. The gas flow was 30 mL/min.

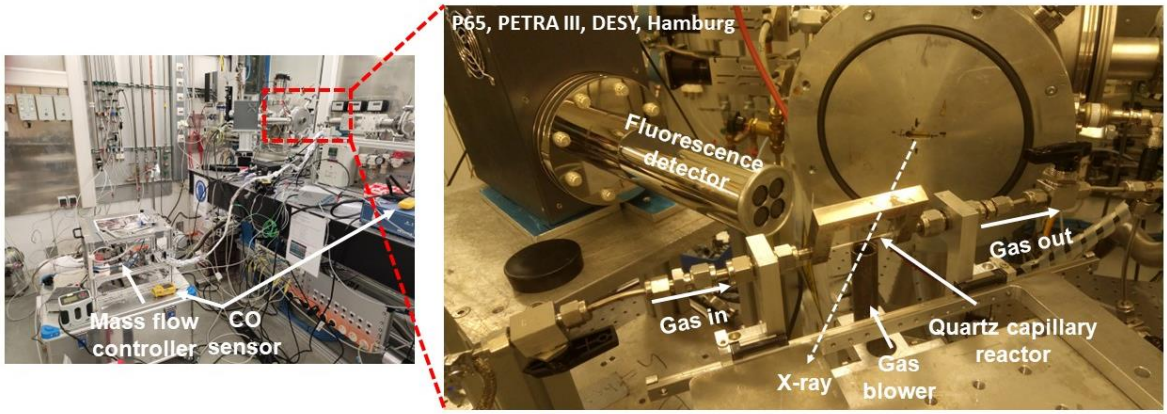

Figure S15. Overview of experimental set-up for *in-situ* XAS studies at P65, PETRA III, DESY, Hamburg, Germany. A back pressure regulator was installed at the gas outlet to regulate the pressure. To ensure safety inside the experimental hutch, CO sensors were installed at various locations.

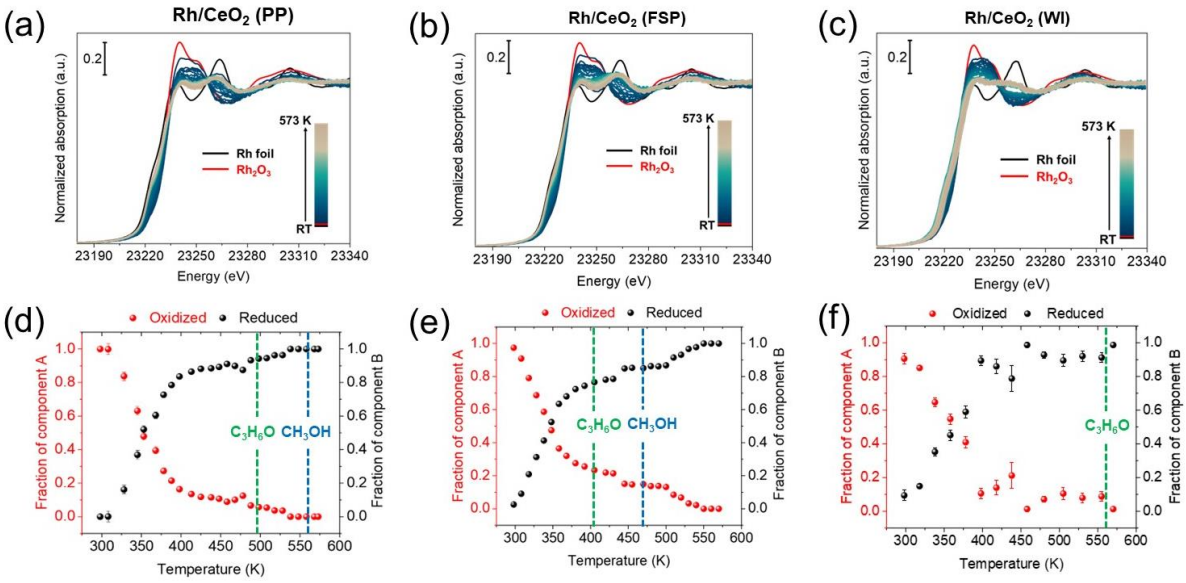

(g)

m/z value (atomic mass unit)	Compound
2	H_2
27 and 28	ethylene
28 and 16	CO
31 and 32	CH_3OH (methanol)
45 and 46	C_2H_5OH (ethanol)
57 and 58	C_3H_6O (propanal)

Figure S16. *In-situ* XANES spectra at the Rh K-edge of Rh/CeO_2 catalysts synthesized by different methods((a)-(c)) and the fraction of component derived from linear combination fitting ((e)-(h)) during hydroformylation of ethylene are shown. (g) represents the m/z value of the fragmentation pattern of various compounds monitored via an online mass spectrometer. PP, FSP and WI stands for precipitation, flame spray pyrolysis and wet impregnation respectively.

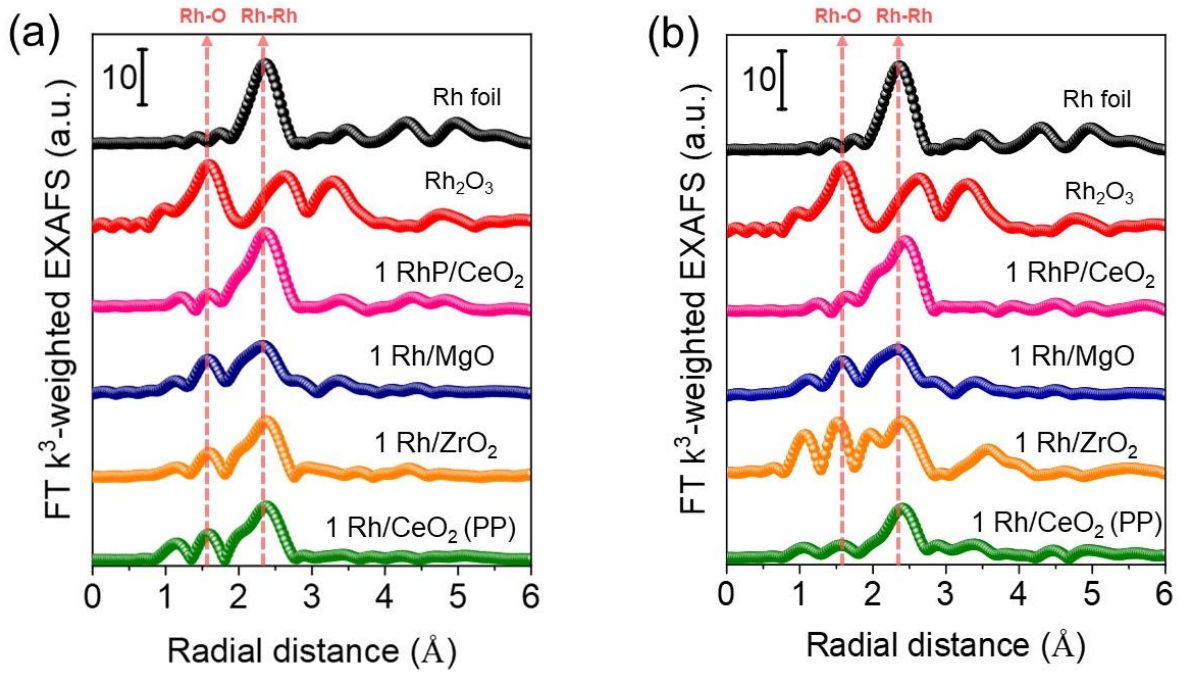

Figure S17. Fourier transformed k^3-weighted EXAFS spectra after (a) hydroformylation reaction of ethylene and (b) CO hydrogenation reaction. Dotted arrow lines are a guide to the eye to show Rh-O and Rh-Rh shell without phase correction.

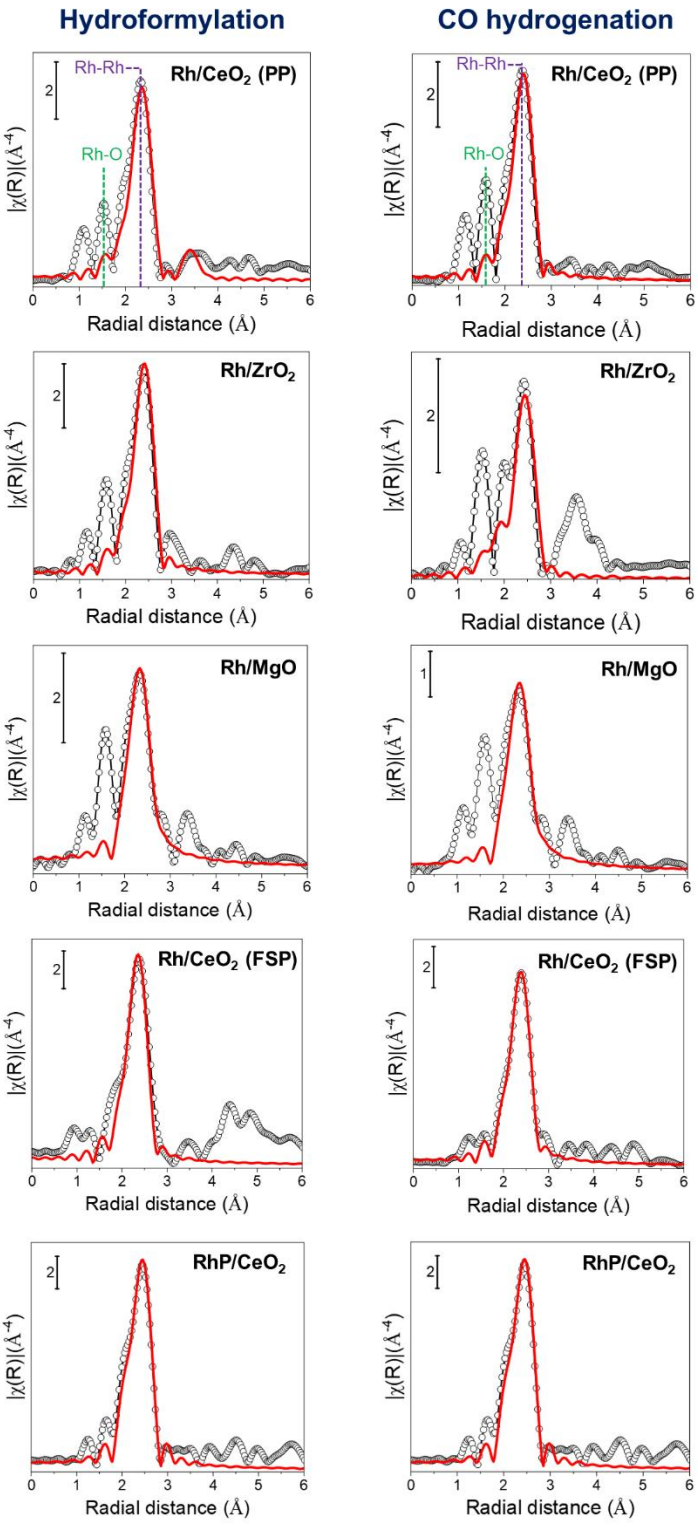

Figure S18. Magnitude (open black circle) of the k^3-weighted EXAFS spectra and the corresponding fit (continuous red line) of catalysts after hydroformylation of ethylene (left) and CO hydrogenation reaction (right). The window considered for fit was between 2-3.1 Å. PP and FSP stand for precipitation and flame spray pyrolysis.

Table S5. Structural parameters derived from EXAFS fitting. The k and radial distance (R) values considered for the fit were 3-12 $Å^{-1}$ and 2.0-3.0 Å respectively. Amplitude reduction factor, S_o^2 was derived from the fit of the metallic Rh foil. The value of S_o^2 was set to be 0.9.

Catalyst	Reaction	Energy shift, E_o (eV)	Scattering path	CN	Radial distance, R (Å)	Debye Waller factor, $\sigma^2(Å^2)$	r-factor
Rh/CeO_2	$CO+C_2H_4+H_2$	-11.4 ±1.6	Rh-Rh	5.5 ±1.1	2.694±0.011	0.0094±0.0016	0.034
Rh/ZrO_2	$CO+C_2H_4+H_2$	-8.3 ±1.4	Rh-Rh	4.7 ±0.9	2.724±0.011	0.0085±0.0016	0.051
Rh/MgO	$CO+C_2H_4+H_2$	-15.4 ±4.5	Rh-Rh	1.2±0.6	2.694±0.017	0.0027±0.0025	0.070
RhP/CeO_2	$CO+C_2H_4+H_2$	-7.3 ±1.1	Rh-Rh	6.0±0.9	2.684±0.007	0.0056±0.0010	0.018
Rh/CeO_2 (FSP)	$CO+C_2H_4+H_2$	-9.1 ±1.4	Rh-Rh	6.3±1.3	2.677±0.009	0.0073±0.0014	0.019
Rh/CeO_2	$CO+H_2$	-7.8 ±1.8	Rh-Rh	4.4 ±1.1	2.711 ± 0.013	0.0084±0.0020	0.024
Rh/ZrO_2	$CO+H_2$	-8.9 ±2.5	Rh-Rh	5.1 ±1.8	2.738±0.028	0.0140±0.0039	0.082
Rh/MgO	$CO+H_2$	-13.3 ±5.3	Rh-Rh	1.1 ±0.6	2.703±0.021	0.0025±0.0031	0.088
RhP/CeO_2	$CO+H_2$	-1.9 ±1.2	Rh-Rh	6.0 ±1.1	2.697±0.009	0.0063±0.0013	0.015
Rh/CeO_2 (FSP)	$CO+H_2$	-8.6 ±1.1	Rh-Rh	4.9±0.8	2.706±0.007	0.0065±0.0011	0.010

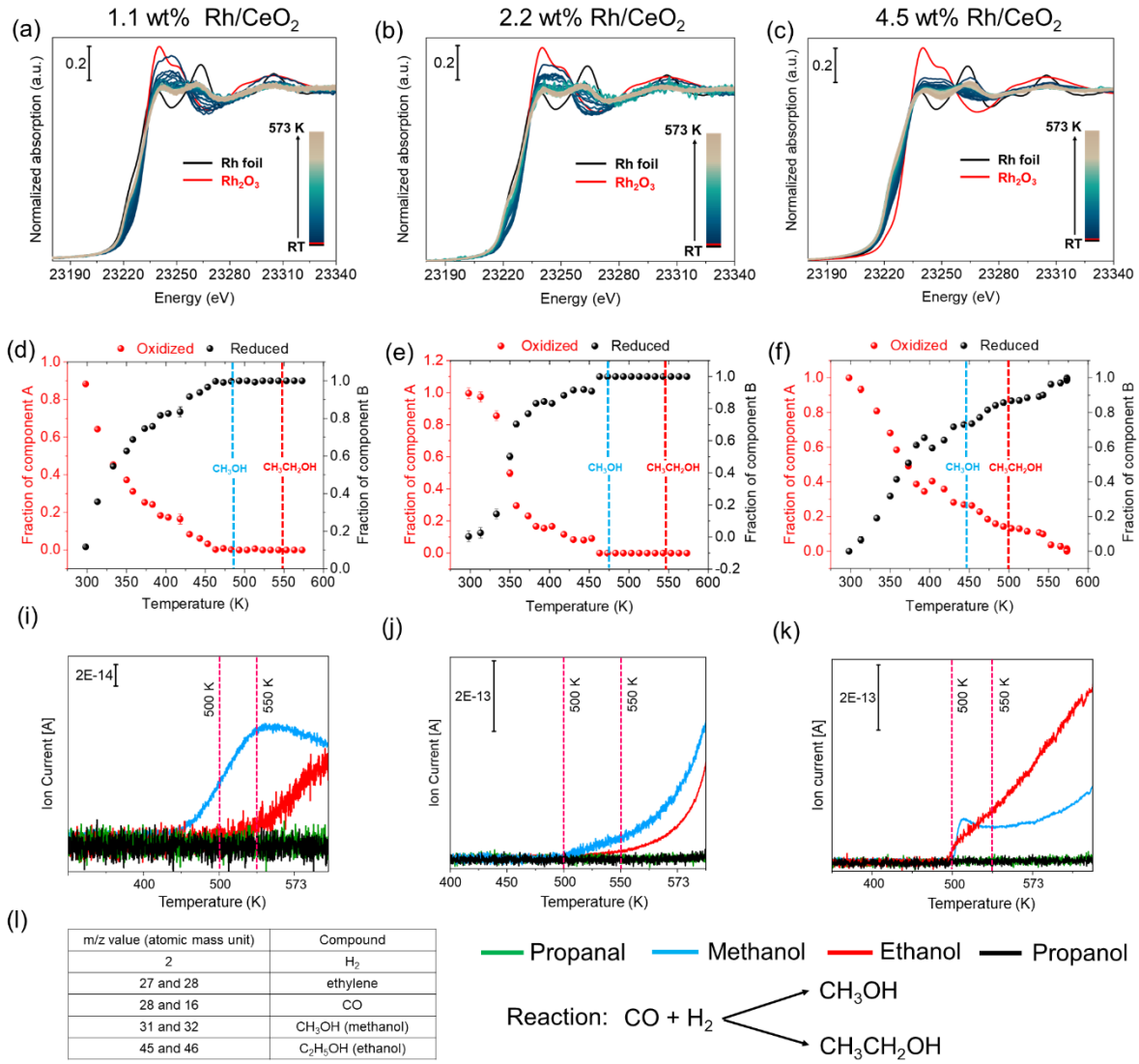

Figure S19. (a)-(c) *In-situ* XANES spectra at the Rh K-edge of Rh/CeO_2 catalysts with different Rh loadings (1.1, 2.2 and 4.5 wt%) during CO hydrogenation reaction and (d)-(f) corresponding fraction of Rh component (oxidized and reduced) derived from linear combination fitting (LCF). (g) represents the m/z value of the fragmentation pattern of various compounds monitored via an online mass spectrometer.

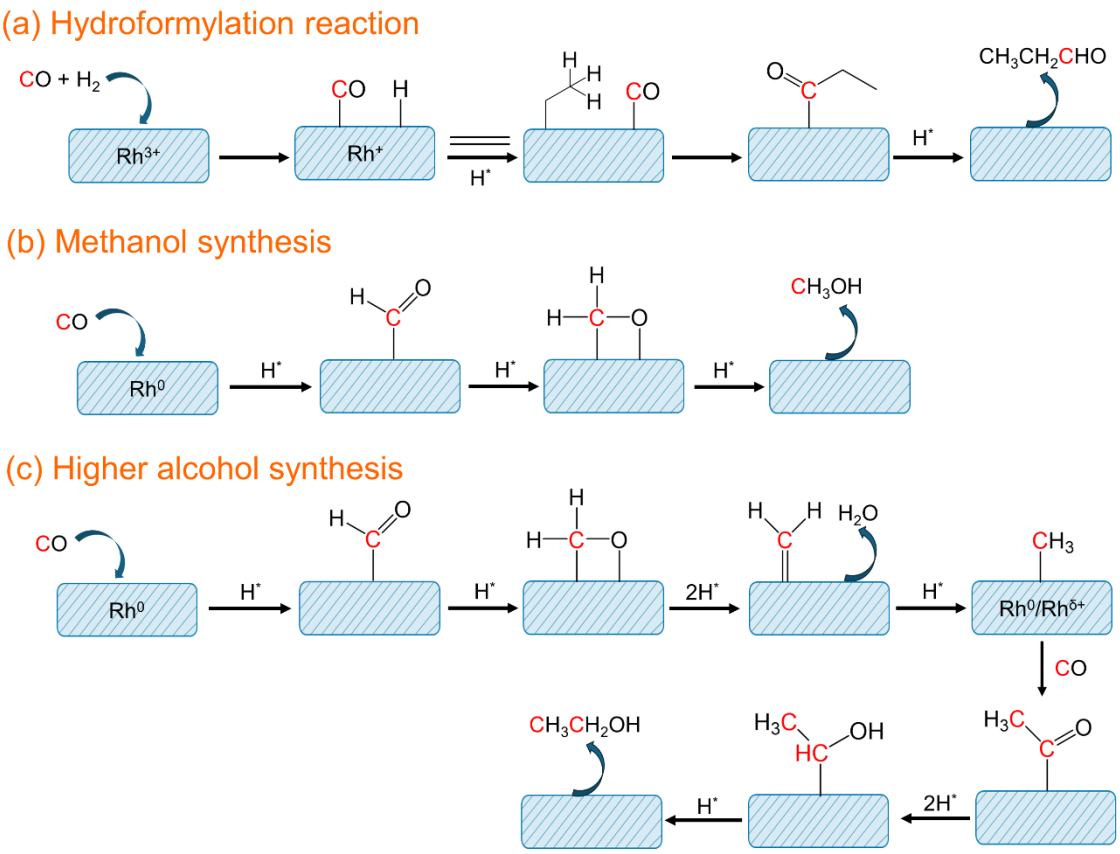

Figure S20. Schematics of three different mechanistic pathways (a) Hydroformylation reaction, (b) Methanol synthesis, and (c) Higher alcohol synthesis over Rh catalyst are shown.

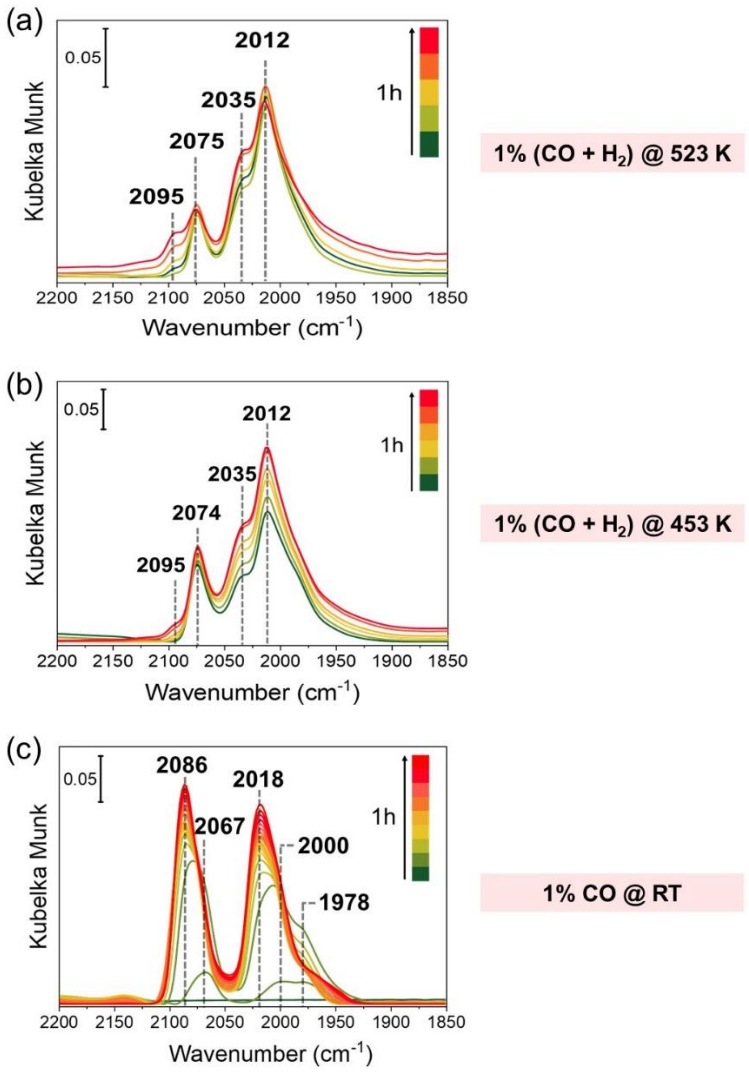

Figure S21. *In-situ* DRIFTS spectra collected under various conditions of the catalyst synthesized via the wetness impregnation method. (a) 1% (CO + H_2) at 523 K (b) 1% (CO + H_2) at 453 K and (c) 1% CO at room temperature.

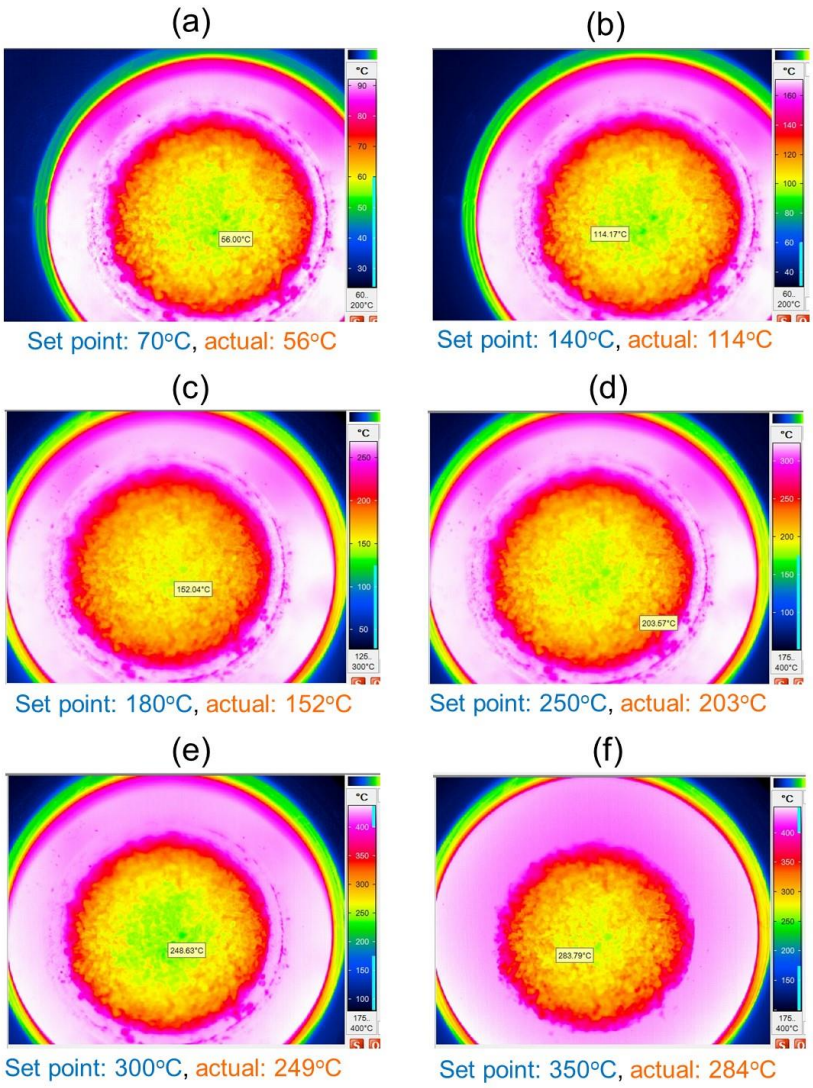

Figure S22. (a)-(f) Temperature calibration between room temperature up to 573 K on the catalyst surface with Infra-red camera under Ar flow at a rate of 40 mL/min. The value at the centre of the catalyst was taken into consideration. Average of 3 measurements were performed. It is evident that at high temperature (573 K), there is a significant difference in temperature (> 100 K) at the centre of the catalyst bed and at the edge. This is critical for designing operando experiments. The temperatures (°C) recorded are shown in the images. A sieve fraction of 100-200 µm of the catalysts was used.

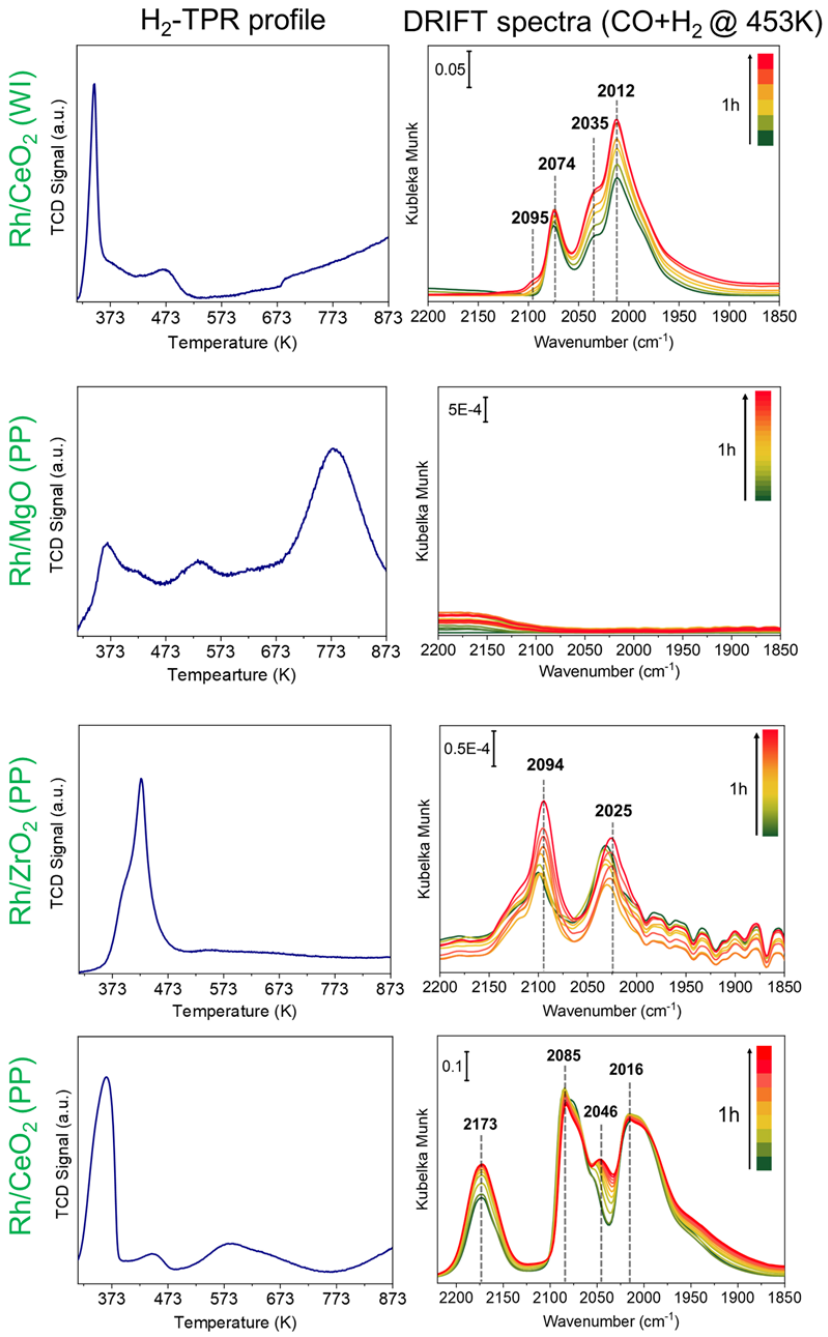

Figure S23. H_2-temperature program reduction (TPR) profile (left) and DRIFT spectra (right) at 453 K with CO + H_2 gas mixture over Rh/CeO_2, Rh/ZrO_2, and Rh/MgO catalysts. PP and WI stand for precipitation and wet impregnation.

Bibliographic references & notes

1. B. B. Sarma, J. Jelic, D. Neukum, D. E. Doronkin, X. Huang, S. Bernart, F. Studt and J.-D. Grunwaldt, Tracking and Understanding Dynamics of Atoms and Clusters of Late Transition Metals with In-Situ DRIFT and XAS Spectroscopy Assisted by DFT, *J. Phys. Chem. C*, 2023, **127**, 3032-3046.
2. E. Welter, R. Chernikov, M. Herrmann and R. Nemausat, A beamline for bulk sample X-ray absorption spectroscopy at the high brilliance storage ring PETRA III, *AIP Conf. Proc.*, 2019, **2054**, 040002.
3. A. Zimina, K. Dardenne, M. A. Denecke, D. E. Doronkin, E. Huttel, H. Lichtenberg, S. Mangold, T. Pruessmann, J. Rothe, T. Spangenberg, R. Steininger, T. Vitova, H. Geckeis and J.-D. Grunwaldt, CAT-ACT—A new highly versatile X-ray spectroscopy beamline for catalysis and radionuclide science at the KIT synchrotron light facility ANKA, *Rev. Sci. Ins.*, 2017, **88**.
4. B. Ravel and M. Newville, ATHENA, ARTEMIS, HEPHAESTUS: data analysis for X-ray absorption spectroscopy using IFEFFIT, *J Syn. Rad.*, 2005, **12**, 537-541.
5. S. Calvin, XAFS for everyone, *CRC Press Taylor & Francis Group*, 2013.
6. J. J. Rehr, J. J. Kas, M. P. Prange, A. P. Sorini, Y. Takimoto and F. Vila, Ab initio theory and calculations of X-ray spectra, *Comptes Rendus Physique*, 2009, **10**, 548-559.
7. Y. Abe, K. Kato, M. Kawamura and K. Sasaki, Rhodium and Rhodium Oxide Thin Films Characterized by XPS, *Sur. Sci. Spectra*, 2002, **8**, 117-125.
8. L. S. Kibis, A. I. Stadnichenko, S. V. Koscheev, V. I. Zaikovskii and A. I. Boronin, XPS Study of Nanostructured Rhodium Oxide Film Comprising Rh^{4+} Species, *J. Phys. Chem. C*, 2016, **120**, 19142-19150.
9. S. Suárez, M. Yates, A. L. Petre, J. A. Martín, P. Avila and J. Blanco, Development of a new Rh/TiO_2–sepiolite monolithic catalyst for N_2O decomposition, *Appl. Catal. B: Env.*, 2006, **64**, 302-311.
10. A. Talo, J. Lahtinen and P. Hautojärvi, An XPS study of metallic three-way catalysts: The effect of additives on platinum, rhodium, and cerium, *Appl. Catal. B: Env.*, 1995, **5**, 221-231.
11. C. Yang and C. W. Garl, Infrared Studies of Carbon Monoxide Chemisorbed on Rhodium, *J. Phys. Chem.*, 1957, **61**, 1504-1512.
12. C. A. Rice, S. D. Worley, C. W. Curtis, J. A. Guin and A. R. Tarrer, The oxidation state of dispersed Rh on Al2O3, *J. Chem. Phys.*, 1981, **74**, 6487-6497.
13. S. S. C. Chuang, R. W. Stevens and R. Khatri, Mechanism of C2+ oxygenate synthesis on Rh catalysts, *Top. Catal.*, 2005, **32**, 225-232.
14. J. C. Matsubu, V. N. Yang and P. Christopher, Isolated Metal Active Site Concentration and Stability Control Catalytic CO_2 Reduction Selectivity, *J. Am. Chem. Soc.*, 2015, **137**, 3076-3084.
15. Y. Tang, C. Asokan, M. Xu, G. W. Graham, X. Pan, P. Christopher, J. Li and P. Sautet, Rh single atoms on TiO_2 dynamically respond to reaction conditions by adapting their site, *Nat. Commun.*, 2019, **10**, 4488.
16. M. J. Hülsey, B. Zhang, Z. Ma, H. Asakura, D. A. Do, W. Chen, T. Tanaka, P. Zhang, Z. Wu and N. Yan, In situ spectroscopy-guided engineering of rhodium single-atom catalysts for CO oxidation, *Nat. Commun.*, 2019, **10**, 1330.
17. R. Lang, T. Li, D. Matsumura, S. Miao, Y. Ren, Y.-T. Cui, Y. Tan, B. Qiao, L. Li, A. Wang, X. Wang and T. Zhang, Hydroformylation of Olefins by a Rhodium Single-Atom Catalyst with Activity Comparable to $RhCl(PPh_3)_3$, *Angew. Chem. Int. Ed.*, 2016, **55**, 16054-16058.
18. Y. Zheng, Q. Wang, Q. Yang, S. Wang, M. J. Hülsey, S. Ding, S. Furukawa, M. Li, N. Yan and X. Ma, Boosting the Hydroformylation Activity of a Rh/CeO_2 Single-Atom Catalyst by Tuning Surface Deficiencies, *ACS Catal.*, 2023, **11**, 7243–7255.
19. D. Wu, S. Liu, M. Zhong, J. Zhao, C. Du, Y. Yang, Y. Sun, J. Lin, S. Wan, S. Wang, J. Huang, Y. Yao, Z. Li and H. Xiong, Nature and Dynamic Evolution of Rh Single Atoms Trapped by CeO_2 in CO Hydrogenation, *ACS Catal.*, 2022, **12**, 12253-12267.
20. Y. Kwon, T. Y. Kim, G. Kwon, J. Yi and H. Lee, Selective Activation of Methane on Single-Atom Catalyst of Rhodium Dispersed on Zirconia for Direct Conversion, *J. Am. Chem. Soc.*, 2017, **139**, 17694-17699.

21. L. Wang, W. Zhang, S. Wang, Z. Gao, Z. Luo, X. Wang, R. Zeng, A. Li, H. Li, M. Wang, X. Zheng, J. Zhu, W. Zhang, C. Ma, R. Si and J. Zeng, Atomic-level insights in optimizing reaction paths for hydroformylation reaction over Rh/CoO single-atom catalyst, *Nat. Commun.*, 2016, **7**, 14036.
22. I. Ro, J. Qi, S. Lee, M. Xu, X. Yan, Z. Xie, G. Zakem, A. Morales, J. G. Chen, X. Pan, D. G. Vlachos, S. Caratzoulas and P. Christopher, Bifunctional hydroformylation on heterogeneous Rh-WOx pair site catalysts, *Nature*, 2022, **609**, 287-292.
23. L. Qi, S. Das, Y. Zhang, D. Nozik, B. C. Gates and A. T. Bell, Ethene Hydroformylation Catalyzed by Rhodium Dispersed with Zinc or Cobalt in Silanol Nests of Dealuminated Zeolite Beta, *J. Am. Chem. Soc.*, 2023, **145**, 2911-2929.
24. M. Zhao, C. Li, D. Gómez, F. Gonell, V. M. Diaconescu, L. Simonelli, M. L. Haro, J. J. Calvino, D. M. Meira, P. Concepción and A. Corma, Low-temperature hydroformylation of ethylene by phosphorous stabilized Rh sites in a one-pot synthesized Rh-(O)-P-MFI zeolite, *Nat. Commun.*, 2023, **14**, 7174.
25. H. Miessner, I. Burkhardt, D. Gutschick, A. Zecchina, C. Morterra and G. Spoto, The formation of a well defined rhodium dicarbonyl in highly dealuminated rhodium-exchanged zeolite Y by interaction with CO, *J. Chem. Soc., Faraday Transactions 1: Phys. Chem. in Condensed Phases*, 1989, **85**, 2113-2126.
26. K. I. Hadjiivanov and G. N. Vayssilov, Characterization of oxide surfaces and zeolites by carbon monoxide as an IR probe molecule, 2002.
27. S. M. McClure, M. J. Lundwall and D. W. Goodman, Planar oxide supported rhodium nanoparticles as model catalysts, *Proc. Nat. Acad. Sci.*, 2011, **108**, 931-936.
28. G. Zakem and P. Christopher, Active Site Entropy of Atomically Dispersed Rh/Al_2O_3 Catalysts Dictates Activity for Ethylene Hydroformylation, *ACS Catal.*, 2023, **13**, 5502-5515.